Published in final edited form as:

Sci Transl Med. 2017 September 13; 9(407): . doi:10.1126/scitranslmed.aad4000.

Endothelial APLNR regulates tissue fatty acid uptake and is essential for apelin's glucose-lowering effects

Cheol Hwangbo[1,*], **Jingxia Wu**[1,*], **Irinna Papangeli**[1], **Takaomi Adachi**[1], **Bikram Sharma**[2], **Saejeong Park**[1], **Lina Zhao**[1], **Hyekyung Ju**[1], **Gwang-woong Go**[1], **Guoliang Cui**[3], **Mohammed Inayathullah**[4], **Judith K. Job**[4], **Jayakumar Rajadas**[4], **Stephanie L. Kwei**[5], **Ming O. Li**[6], **Alan R. Morrison**[1], **Thomas Quertermous**[7], **Arya Mani**[1], **Kristy Red-Horse**[2], and **Hyung J. Chun**[1,†]

[1]Yale Cardiovascular Research Center, Section of Cardiovascular Medicine, Yale School of Medicine, New Haven, CT 06511, USA

[2]Department of Biology, Stanford University, Stanford, CA 94304, USA

[3]Department of Immunobiology, Yale School of Medicine, New Haven, CT 06511, USA

[4]Biomaterials and Advanced Drug Delivery Laboratory, Stanford University, Stanford, CA 94304, USA

[5]Section of Plastic and Reconstructive Surgery, Yale School of Medicine, New Haven, CT 06511, USA

[6]Immunology Program, Memorial Sloan Kettering Cancer Center, New York, NY 10065, USA

[7]Division of Cardiovascular Medicine, Stanford University, Stanford, CA 94304, USA

Abstract

Treatment of type 2 diabetes mellitus continues to pose an important clinical challenge, with most existing therapies lacking demonstrable ability to improve cardiovascular outcomes. The atheroprotective peptide apelin (APLN) enhances glucose utilization and improves insulin sensitivity. However, the mechanism of these effects remains poorly defined. We demonstrate that the expression of APLNR (APJ/AGTRL1), the only known receptor for apelin, is predominantly restricted to the endothelial cells (ECs) of multiple adult metabolic organs, including skeletal muscle and adipose tissue. Conditional endothelial-specific deletion of *Aplnr* (*Aplnr*^{ECKO}) resulted in markedly impaired glucose utilization and abrogation of apelin-induced glucose lowering. Furthermore, we identified in-activation of Forkhead box protein O1 (FOXO1) and inhibition of endothelial expression of fatty acid (FA) binding protein 4 (FABP4) as key

†Corresponding author. hyung.chun@yale.edu.
*These authors contributed equally to this work.

Author contributions: C.H., J.W., and H.J.C. designed the research. C.H., J.W., I.P., B.S., S.P., L.Z., T.A., H.J., G.-w.G., G.C., and A.R.M. performed the experiments. M.I., J.K.J., and J.R. generated and provided the apelin formulations. S.L.K. collected and prepared the human samples. M.O.L. generated and provided the *Foxo1*$^{fl/fl}$ mouse line. T.Q. generated and provided the *Apln*$^{-/-}$ and *Aplnr*$^{fl/fl}$ mouse lines. M.O.L., T.Q., A.R.M., A.M., and K.R.-H. assisted with the data analyses and review of the manuscript. C.H., J.W., I.P., and H.J.C. prepared the figures and wrote the manuscript.

Competing interests: The authors declare that they have no competing interests.

Data and materials availability: The gene expression profile data have been deposited into the GEO data set (accession no. GSE67390). *Cdh5*(PAC)-CreERT2 mice are available from R. Adams under a material agreement with Cancer Research UK. *Foxo1*$^{fl/fl}$ mice are available from M.O.L. under a material agreement with Memorial Sloan Kettering Cancer Center.

downstream signaling targets of apelin/APLNR signaling. Both the *Apln*$^{-/-}$ and *Aplnr*^{ECKO} mice demonstrated increased endothelial FABP4 expression and excess tissue FA accumulation, whereas concurrent endothelial *Foxo1* deletion or pharmacologic FABP4 inhibition rescued the excess FA accumulation phenotype of the *Apln*$^{-/-}$ mice. The impaired glucose utilization in the *Aplnr*^{ECKO} mice was associated with excess FA accumulation in the skeletal muscle. Treatment of these mice with an FABP4 inhibitor abrogated these metabolic phenotypes. These findings provide mechanistic insights that could greatly expand the therapeutic repertoire for type 2 diabetes and related metabolic disorders.

INTRODUCTION

Our understanding of the role of the mature endothelium continues to evolve, with recognition that it serves as a key regulator of physiologic and pathologic processes through its signals to the surrounding organs (1, 2). The network of endothelial capillaries coordinates fluid and nutrient transport between the circulation and the target tissues and has a key role in the control of energy balance. In particular, fatty acids (FAs) must cross the endothelial barrier for storage in the adipose tissues and for energy utilization in the skeletal and cardiac muscles. Although FAs can serve as a crucial energy source, excess FA deposition may have deleterious effects on the target tissues, such as impaired glucose utilization and insulin resistance (3–7).

Heterotrimeric guanine nucleotide–binding protein–coupled receptor signaling mediated by apelin and APLNR has critical roles in developmental angiogenesis and protective effects in multiple vascular disease models, including atherosclerosis (8–11). Although metabolic effects such as improvement in insulin sensitivity and decreased adiposity have been attributed to apelin (12, 13), the downstream mechanisms of apelin/APLNR signaling remain inadequately defined. Here, we demonstrate that in adult metabolic tissues, APLNR expression is predominantly constrained to the endothelium. We found that apelin serves as a key inhibitor of FA transport across the endothelial layer, as shown by excess FA transport and accumulation in target tissues of mice with disrupted apelin signaling. This process is critically dependent on apelin-induced inactivation of the transcription factor Forkhead box protein O1 (FOXO1) in the endothelium, which subsequently causes marked inhibition of endothelial FA binding protein 4 (FABP4) expression. Our findings identify apelin signaling as an endothelial-based therapeutic target that may concurrently improve glycemic control while reversing endothelial dysfunction, providing notable advantages over traditional and newer classes of antidiabetic agents that fail to improve cardiovascular outcomes (14–19).

RESULTS

APLNR expression is restricted to the endothelium of adult tissues

Given the absence of a robust antibody to detect APLNR expression, we used two independent techniques to characterize APLNR expression in adult tissues. First, we performed in situ hybridization in human skeletal muscle and white adipose tissue (WAT) and found that *APLNR* expression is restricted predominantly to the endothelial cells (ECs) (Fig. 1A and fig. S1A). Second, we evaluated APLNR expression using a recently described

mouse line harboring an inducible Cre recombinase under the control of the *Aplnr* enhancer/promoter (*Aplnr*^{CreER}) on a *Rosa*^{mTmG} reporter background (20, 21). In adult skeletal muscle, WAT, and brown adipose tissue (BAT), APLNR expression was again predominantly restricted to the endothelium (vessel diameters of <~50 μm), as confirmed by costaining for the endothelial marker vascular endothelial cadherin (VE-cadherin) (Fig. 1B), although not all ECs expressed APLNR, including those in muscularized vessels (fig. S1B). We next determined *Aplnr* expression in tissue homogenates of mouse skeletal muscle, WAT, and BAT, and compared it to its expression in isolated ECs from the respective tissues. Consistent with the tissue sections, we found that mRNA expression of *Aplnr* in the isolated ECs is ~10- to ~150-fold higher than in the whole tissues (Fig. 1C).

Endothelial APLNR is critical for apelin signaling and its glucose-lowering effects

Given the restricted expression profile of APLNR, we investigated the role of ECs in mediating apelin's downstream signaling. Skeletal muscle cell preparations subjected to EC depletion using negative cell sorting with anti-CD31 antibody failed to respond to exogenous apelin, as demonstrated by the absence of increased AKT or 5′-adenosine monophosphate–activated protein kinase α (AMPKα) phosphorylation, whereas skeletal muscle cell preparations treated with control immunoglobulin G (IgG) antibody demonstrated robust response to apelin (Fig. 2A). Next, we determined the effect of apelin treatment in conditional, endothelial-specific *Aplnr*-deficient mice (*Aplnr*^{ECKO}) by crossing tamoxifen-inducible, *Cdh5*(PAC)-CreERT2 miceto *Aplnr*$^{fl/fl}$ mice (22, 23). Apelin treatment of skeletal muscle from *Aplnr*^{ECKO} mice failed to induce AKT or AMPKα phosphorylation, further supporting the endothelial basis of this signaling (Fig. 2B). Moreover, phosphorylation of endothelial nitric oxide synthase (eNOS) was also impaired in response to apelin stimulation of skeletal muscle from *Aplnr*^{ECKO} mice (Fig. 2B).

We further investigated the metabolic phenotype of *Aplnr*^{ECKO} mice against *Aplnr*$^{fl/fl}$ controls. The body weights were comparable between the two groups (29.56 ± 0.19 g for control versus 29.53 ± 0.94 g for *Aplnr*^{ECKO}, not significant), and body composition analysis found no significant difference in the fat mass or muscle mass of these mice compared to controls (fig. S2). *Aplnr*^{ECKO} mice had increased blood glucose concentrations compared to control mice when subjected to intraperitoneal glucose tolerance test (IPGTT) (Fig. 2C). Moreover, whereas apelin injection in control mice resulted in a reduction in glucose levels in IPGTT, apelin injection in *Aplnr*^{ECKO} mice failed to elicit any changes in their glucose concentrations (Fig. 2D). In addition, *Aplnr*^{ECKO} mice displayed impaired response to insulin tolerance testing compared to control mice (Fig. 2E). Basal concentrations of circulating insulin in the *Apln*$^{-/-}$, *Aplnr*$^{-/-}$, and *Aplnr*^{ECKO} mice were not significantly different from their respective control groups (fig. S3). Moreover, the serum concentration of adiponectin, which can also affect glucose utilization, was not significantly altered in *Aplnr*^{ECKO} mice (fig. S4).

We sought to further evaluate the mechanism of impaired glucose utilization in *Aplnr*^{ECKO} mice. First, to examine whether the difference in glucose utilization was due to changes in tissue blood flow, we conducted a laser Doppler scan to determine the resting hindlimb blood flow. We found no difference between control and *Aplnr*^{ECKO} mice under basal

conditions (fig. S5, A and B). Second, we tested whether apelin stimulation can affect transendothelial glucose or insulin transport. Pretreatment of human coronary microvascular ECs (HCMECs) with apelin had no effect on transendothelial glucose or insulin transfer (fig. S6, A and B). We also evaluated the endogenous expression of apelin, via lacZ staining of *Apln*$^{+/lacz}$ mice (24). Apelin, similar to APLNR, was expressed predominantly in the ECs of skeletal muscles, WAT, and BAT (Fig. 2F). In mice that were subjected to a high-fat diet, developed weight gain, and impaired glucose utilization (fig. S7, A and B), there was a decrease in apelin expression, as determined by both lacZ staining and quantitative polymerase chain reaction (PCR) analysis (Fig. 2, F and G). We also tested whether high glucose conditions (30 mM) could affect *APLN* expression in cultured HCMECs and found no significant change in apelin expression (fig. S8).

Apelin induces endothelial FOXO1 inactivation

The expression profile of APLNR in human tissues, the *Aplnr*^{CreER} reporter mouse strain, and our metabolic findings in the *Aplnr*^{ECKO} mice all suggested that the ECs are likely the primary determinants of apelin signaling in adult tissues. We sought to investigate endothelial-based targets of apelin that are integral to the demonstrated metabolic phenotype. A well-described target of AKT is the transcription factor FOXO1, which belongs to the forkhead family of transcription factors with important roles in metabolism (25–27). We found that apelin can robustly promote FOXO1 phosphorylation in ECs (Fig. 3, A and B), in conjunction with its cytoplasmic translocation (Fig. 3C). EC pretreatment with either Wortmannin or LY-294002, inhibitors of the phosphoinositide 3-kinase pathway, abrogated apelin-mediated FOXO1 phosphorylation (Fig. 3D).

FABP4 is a key target of EC-based apelin-FOXO1 signaling

Given the robust phosphorylation and inactivation of FOXO1 by apelin and the known importance of FOXO1 in endothelial transcriptional regulation (28), we sought to identify its transcriptional targets that are also regulated by apelin/APLNR signaling. We conducted gene expression profiling analysis to identify transcripts that are inversely regulated by *APLN/APLNR* knockdown and *FOXO1* knockdown in human umbilical vein endothelial cells (HUVECs) [fig. S9; GEO (Gene Expression Omnibus) data set accession no. GSE67390]. We found that the two transcripts that were the most robustly inversely regulated were *C10orf10* (*DEPP*), a transcript preferentially expressed in the developing arterial ECs without a well-described function (29), and *FABP4*, an FA transport protein that was originally identified in adipocytes but also described to be expressed in ECs (30, 31). A closely related gene, *FABP5*, was not significantly affected by *APLN/APLNR* knockdown in the expression profiling analysis. Moreover, we found a strong correlation between the genes differentially regulated in our gene expression profile in response to *FOXO1* knockdown and a previous study of *FOXO1/ FOXO3A* combined knockdown (table S1) (28). Of these genes, only a subset was inversely regulated by *APLN/APLNR* knockdown, suggesting that although FOXO1 regulates a wide spectrum of EC genes, other upstream mechanisms, independent of apelin/APLNR, are also important in regulating FOXO1 activity.

We chose to further investigate the role of FABP4 as a key metabolic target of endothelial apelin/FOXO1 signaling. FABP4 was increased by *APLN* knockdown and decreased in response to *FOXO1* knockdown; moreover, concurrent knockdown of *APLN* and *FOXO1* abrogated *APLN* knockdown–mediated FABP4 induction, further supporting the hypothesis that FOXO1 functions downstream of apelin in regulating FABP4 (Fig. 3E and fig. S10). We also tested whether a previously described transcriptional regulator of FABP4, peroxisome proliferator– activated receptor γ (PPARγ) (32), may be involved in controlling FABP4 downstream of apelin. We found that *APLN* knockdown–mediated increase in *FABP4* was not affected by concurrent *PPARG* knockdown, suggesting that PPARγ is not a direct downstream target of apelin signaling (fig. S11).

To validate our findings in vivo, we used $Apln^{-/-}$ and $Aplnr^{ECKO}$ mice (22) and mice with conditional, endothelial-specific deletion of *Foxo1* ($Foxo1^{ECKO}$) (23, 33). $Apln^{-/-}$ and $Aplnr^{ECKO}$ mice displayed increased expression of FABP4 in isolated ECs from skeletal muscle (Fig. 3F). In contrast, FABP4 expression in the ECs of $Foxo1^{ECKO}$ mice was decreased compared to littermate controls (Fig. 3F). Increased endothelial FABP4 expression was also demonstrated in skeletal muscles of $Apln^{-/-}$ mice by immunofluorescence staining; this increase was abrogated in the $Apln^{-/-}$:$Foxo1^{ECKO}$ mice (fig. S12). Next, we subjected wild-type C57Bl/6 mice to concurrent high-fat diet and continuous infusion of apelin. We found that after 1 week, the high-fat diet–fed mice in the vehicle group had worse glucose utilization, as determined by IPGTT, compared to those receiving apelin infusion (fig. S13). This was associated with decreased expression of FABP4 in the skeletal muscle homogenates of apelin-treated mice (fig. S14).

FA uptake and transport across the endothelial layer are regulated by apelin signaling

Given the regulation of FABP4 by the apelin/FOXO1 signaling cascade in the endothelium and its known role in FA binding and transport (34), we examined whether FA uptake and transfer across the endothelium may be targeted by this signaling cascade. First, we used HCMECs to test the effects of either apelin stimulation or *APLNR* knockdown on endothelial FA uptake. BODIPY 558/568C12 (BODIPY) uptake was decreased when ECs were stimulated with apelin (Fig. 4A), whereas *APLNR* knockdown resulted in increased BODIPY uptake (Fig. 4B). Similar effects were also demonstrated in HUVECs (fig. S15A). Next, we used ECs plated to confluence on Transwell inserts to evaluate the transfer of BODIPY across the EC layer. We found that pretreatment with apelin decreased BODIPY transfer across the cell layer, whereas knockdown of *APLNR* increased it in both HCMECs (Fig. 4, C and D) and HUVECs (fig. S15B). Furthermore, we sought to investigate whether the enhanced FA transfer due to disruption of apelin/APLNR signaling can be abrogated by BMS309403, which is a potent FABP4 inhibitor (35, 36). We found that BMS309403 effectively reversed the increased FA transfer observed in ECs subjected to combined *APLN* and *APLNR* knockdown in a dose-dependent manner in both HCMECs (Fig. 4E) and HUVECs (fig. S15C).

Apln$^{-/-}$ mice develop excess FA accumulation that is rescued by deletion of endothelial *Foxo1* or FABP4 inhibition

We next proceeded to recapitulate our findings in vivo. *Apln*$^{-/-}$ mice demonstrated an increase in FA accumulation in multiple metabolically active tissues, including the heart, skeletal muscle, liver, and BAT, after these animals were treated with ^{14}C-labeled oleic acid (^{14}C-OA) by oral gavage (Fig. 4F). Skeletal muscles of *Apln*$^{-/-}$ mice demonstrated increased oil red O staining compared to wild-type littermates (Fig. 4G). Conversely, *Foxo1*^{ECKO} mice had reduced FA accumulation (fig. S16). These changes were in the absence of any significant difference in the circulating serum concentrations of ^{14}C-OA in *Apln*$^{-/-}$ and *Foxo1*^{ECKO} mice, suggesting that the intestinal lymphatic absorption was not affected in these mice (fig. S17) (37). We evaluated the serum concentrations of ^{14}C-OA in the *Aplnr*^{ECKO} mice up to 24 hours after oral administration and found no significant difference from the control group (fig. S18).

To further validate the relevance of FOXO1 and FABP4 as key downstream endothelial targets of apelin/APLNR signaling in the regulation of FA uptake, we investigated the effects of either (i) combined *Apln* and endothelial *Foxo1* deletion (*Apln*$^{-/-}$:*Foxo1*^{ECKO}) or (ii) treatment of *Apln*$^{-/-}$ mice with BMS309403 as potential strategies to rescue the excess FA uptake observed in *Apln*$^{-/-}$ mice. First, we found that impaired glucose utilization in *Apln*$^{-/-}$ mice, as demonstrated in IPGTT, was improved in the *Apln*$^{-/-}$:*Foxo1*^{ECKO} mice (Fig. 5A). The *Apln*$^{-/-}$:*Foxo1*^{ECKO} mice also had decreased staining for oil red O in their skeletal muscles compared to *Apln*$^{-/-}$ mice (Fig. 5B). Finally, we found normalization of ^{14}C-OA uptake in *Apln*$^{-/-}$:*Foxo1*^{ECKO} mice compared to *Apln*$^{-/-}$ mice (Fig. 5C). Treatment of *Apln*$^{-/-}$ mice with BMS309403 decreased ^{14}C-OA uptake but had negligible effect on wild-type littermates (Fig. 5D).

Impaired glucose utilization of *Aplnr*^{ECKO} mice can be rescued by FABP4 inhibition

To further evaluate the metabolic effects of endothelial apelin/APLNR signaling, we characterized the *Aplnr*^{ECKO} mice. Similar to what we observed in the *Apln*$^{-/-}$ mice, we found increased FA accumulation in multiple tissues of *Aplnr*^{ECKO} mice that received ^{14}C-OA by oral gavage (Fig. 6A), in conjunction with increased oil red O staining in skeletal muscles (Fig. 6B). Analysis of skeletal muscle FA components and triglycerides was performed and demonstrated that palmitic acid (16:0) and stearic acid (18:0) were elevated, whereas the triglyceride content was unaffected in the *Aplnr*^{ECKO} mice (fig. S19). Given previous data suggesting increased endothelial permeability from disrupted apelin signaling (37), we evaluated for any changes in vascular permeability in the *Aplnr*^{ECKO} mice and found no increase in Evans Blue dye leakage in skeletal muscles and lungs compared to the control littermates (fig. S20). Furthermore, we assessed transendothelial transfer of 70-kDa fluorescein isothiocyanate (FITC)– labeled dextran across a confluent monolayer of HCMECs subjected to *APLN* and *APLNR* knockdown and found no change in endothelial permeability (fig. S21).

To further validate the role of the endothelial apelin/APLNR signaling pathway in regulation of glucose utilization, we tested the efficacy of FABP4 inhibition in restoring the normalization of glucose utilization in the *Aplnr*^{ECKO} mice. Treatment of *Aplnr*^{ECKO} mice

with BMS309403 improved glucose utilization by IPGTT (Fig. 6C), whereas control mice were minimally affected (fig. S22). The improved glucose utilization in $Aplnr^{ECKO}$ mice was associated with decrease in oil red O staining in skeletal muscles (Fig. 6D), further demonstrating the important role of FABP4 as a critical target of endothelial apelin/APLNR signaling.

DISCUSSION

Recent studies focusing on endothelial mechanisms of FA uptake have shed insights into pathways ensuring stringent metabolic control, which can be therapeutically targeted to improve metabolic parameters, such as insulin sensitivity and glucose uptake (38–41). Our findings that (i) endothelial-specific *Aplnr* deletion results in glucose intolerance and failure to respond metabolically to apelin, (ii) apelin is a robust inhibitor of endothelial FOXO1 activity and FABP4 expression, and (iii) genetic or pharmacologic targeting of these downstream targets rescues the metabolic phenotype in $Apln^{-/-}$ or $Aplnr^{ECKO}$ mice demonstrate that the endothelial mechanism described here is a key mediator of apelin's metabolic effects (Fig. 6E). Moreover, our current findings provide mechanistic insights into the previous studies on $Apln^{-/-}$ mice, which have normal weights at baseline but become obese and insulin-resistant in response to high-fat diet (13, 37). Here, we demonstrate two concepts in the role of apelin/APLNR signaling in metabolism. First, our characterization of the $Aplnr^{ECKO}$ mice provides genetic evidence that endothelial apelin signaling is the determinant of its effects on insulin sensitivity and glucose utilization. Second, we show that active endothelial FA uptake and transfer, rather than compromised endothelial permeability, as previously suggested (37), is a critical mechanism controlled by apelin/APLNR signaling through downstream targeting of FOXO1 inhibition and endothelial FABP4 expression. Because our current studies using $Aplnr^{ECKO}$ mice under basal conditions do not demonstrate any perturbation in endothelial permeability, the impact of high-fat diet and other metabolic imbalances on additional downstream targets of apelin/APLNR signaling warrants further evaluation.

Our studies provide a profiling of APLNR expression in adult tissues, which, to date, has been hampered by the lack of a reliable antibody. The combination of in situ hybridization and the use of the $Aplnr^{CreER}$ mouse line demonstrates that APLNR expression is predominantly restricted to the endothelium in adult mice. The restricted expression pattern of APLNR strongly suggests that the endothelial mechanism may be the key driver of apelin's metabolic effects. Given apelin's demonstrated physiologic effects in other organs such as the brain and the heart (42), additional studies using conditional deletion of *Aplnr* will be necessary to examine the cell-specific role of this pathway. Our demonstration of differential ^{14}C-OA uptake at 2 hours in the hearts of $Apln^{-/-}$ mice, which is abrogated by 24 hours, highlights a difference between cardiac FA uptake and utilization compared to those of skeletal muscle. Although investigation of the mechanism for this difference is beyond the scope of the current work, additional knowledge of the disparity in energy utilization will be essential, as we seek to understand the mechanisms of diabetes and associated cardiovascular complications.

Our demonstration of decreased apelin expression in mice subjected to high-fat diet provides support for impaired apelin signaling as an important contributor to the pathogenesis of diabetes and metabolic syndrome. Although clinical studies have attempted to measure circulating apelin concentrations in these conditions, they have been hampered by the lack of reliable assays and the heterogeneity of the studied patient populations (43–45). Additional studies to expand our knowledge of how apelin's transcription and isoform cleavage are regulated, as well as the feasibility of using this pathway for clinical therapies, will be critical, and ongoing clinical trials are already testing the efficacy of augmenting apelin/APLNR signaling in humans (46, 47). Studies demonstrating apelin as a transcriptional target of PPARγ in the lung endothelium (48, 49) provide a potentially important regulatory mechanism that may also be involved in other endothelial beds.

The function of endothelial FOXO factors has been described in both developmental and vascular disease contexts (50–52). Both the global *Foxo1* knockout and the Tie2-Cre–driven endothelial deletion of *Foxo1* result in early embryonic lethality (51, 53). In contrast, mice with combined endothelial deletion of *Foxo1*, *Foxo3a*, and *Foxo4* were viable and were protected against atherosclerosis on the $Ldlr^{-/-}$background (52). Insulin signaling regulates FOXO1 phosphorylation and activity via AKT (54); in turn, endothelial FOXO activation can cause endothelial dysfunction by (i) inhibiting eNOS expression and (ii) promoting negative feedback on insulin signaling (52, 55, 56). Further investigation into how apelin and insulin may converge to synergistically regulate FOXO1 signaling should provide additional insights into these secretory factors that can regulate FOXO1 functions in health and disease. Moreover, AMPK is a downstream target of apelin (9, 57). Although AMPK also regulates the FOXO family of transcription factors (58), understanding the convergence of these molecules as downstream targets of apelin signaling will elucidate the metabolic flexibility afforded by this key pathway.

FABP4 and other proteins involved in FA binding and transport continue to be intensely investigated. Emerging studies have begun to identify the function of these proteins in the ECs (59). Although the exact mechanisms remain to be fully understood, these proteins facilitate the uptake and transport of FA, and their pharmacologic inhibition in experimental models has demonstrated compelling evidence for improvement of atherosclerosis (36), improvement of endothelial dysfunction (60), and amelioration of dyslipidemia (61). Characterization of the FABP4 global knockout mouse has also identified its critical role in promoting insulin resistance (62). Delineation of endothelial FABP4 contribution to this context would be important, as we continue to explore endothelial mechanisms that have profound effects on global metabolic states.

Although our findings of engagement of FOXO1 and FABP4 by apelin/APLNR signaling demonstrate the importance of these factors as key downstream mediators, given the molecular signaling complexities of diabetes and its experimental animal models, cross-talk among multiple signaling pathways, including those that mediate endothelial regulation of FA transport (39, 41), is likely a key determinant in how discrete tissue beds regulate energy and nutrient utilization. Our studies identify an endothelial signaling mechanism that is important for glucose utilization in response to apelin. In an era when approval of antidiabetic drugs does not require demonstrated improvements in cardiovascular outcomes

(18, 19) and aggressive glycemic control with existing therapies fails to correlate with a reduction in cardiovascular comorbidities (14–16), using the endothelial apelin/APLNR signaling paradigm and its robust downstream vasoprotective effects represents an innovative antidiabetic therapeutic strategy (10). Our studies highlight the importance of targeting the FA transport properties of the endothelium as an emerging translational strategy to improve glucose utilization and insulin sensitivity in type 2 diabetes.

MATERIALS AND METHODS

Study design

The main research objectives of these studies were to investigate the mechanisms by which engagement of the apelin/APLNR signaling enhances glucose utilization and increases insulin sensitivity. These studies were conducted using a combination of genetically modified mice and pharmacologic treatments supported by in vitro mechanistic data. The number of animals used in each group for each experiment is reported in the figure legends. The mice used for pharmacologic treatment were assigned randomly once their genotypes were confirmed. The metabolic and FA accumulation studies were analyzed blinded to the genotype or pharmacological treatment. All graphs and numerical values in the figures are presented as means ± SEM.

Study approval

All animal experiments were conducted with approval of the Yale University or Stanford University Institutional Animal Care and Use Committees. Human tissue studies were conducted on discarded, deidentified surgical specimens or on purchased tissue sections (OriGene).

Mice

The *Apln*$^{-/-}$, *Aplnr*^{CreER}:*Rosa*^{mTmG}, *Foxo1*$^{fl/fl}$, *Aplnr*$^{fl/fl}$, and *Cdh5*(PAC)-CreERT2 mice have been previously described (20, 22–24, 33). For *Aplnr*^{CreER}:*Rosa*^{mTmG} mice, 6- to 8-week-old mice were injected with 4 mg of tamoxifen (T5648, Sigma-Aldrich; 10 mg/ml dissolved in 100% ethanol and subsequently in corn oil) intraperitoneally three times at an interval of 2 days to induce recombination. For *Aplnr*^{ECKO} and *Foxo1*^{ECKO} mice, Cre activity was induced in 5-week-old mice by five consecutive intraperitoneal injections of 1 mg of tamoxifen. Gene deletion efficiency was confirmed (figs. S23 and S24). Littermates for the respective conditional knockout mice lacking the Cre driver injected with the same tamoxifen regimen were used as controls. Five weeks after tamoxifen injection, the mice were used for the indicated experiments. For high-fat diet–fed mice, they were given an atherogenic rodent diet (TD-02028, Harlan). Body composition was assessed by ^{1}H magnetic resonance spectroscopy using a Bruker Minispec analyzer (Bruker BioSpin). For laser Doppler flow imaging analysis, the animals were anesthetized and maintained under 2% isoflurane and oxygen flow rate of 1 liter/min. Tissue perfusion of mouse hindlimb was measured by laser Doppler spectroscopy. For the apelin infusion experiment, apelin-13 (Sigma-Aldrich) diluted in phosphate-buffered saline (PBS) or vehicle (PBS only) was continuously infused for 7 days at 2 mg/kg per day by subcutaneous osmotic mini-pump

(model 1004, ALZET) in 8-week-old mice. Miles assay using filtered Evans Blue dye was performed as previously described (63).

Ex vivo treatment with apelin

Mouse soleus muscle was dissected and minced. The muscle was digested with collagenase A (2 mg/ml) with gentle agitation for 45 min at 37°C. The cell suspension was triturated, filtered through 70-μm cell strainers, and then centrifuged. Cells were resuspended with 10 ml of cold PBS containing 0.1% bovine serum albumin (BSA). To remove ECs from the tissue, the cell suspension was incubated for 30 min with Dynabeads (11035, Invitrogen) coated with (i) control IgG (12–371, Millipore) for non–EC-depleting conditions or (ii) antibody against CD31 (553370, BD Pharmingen) for EC-depleting conditions. Dynabeads were then magnetically removed. EC depletion was conducted a total of three times per sample. The skeletal myocytes were resuspended in complete Dulbecco's modified Eagle's medium and stimulated with apelin (1 μM) for 1 hour before protein lysates were prepared.

Cell culture and reagents

HUVECs were purchased from the Yale Vascular Biology and Therapeutics core and cultured in endothelial basal medium-2 (EBM-2) containing the BulletKit supplement (Lonza). Additional HUVECs and HCMECs were purchased from Lonza. HUVECs and HCMECs between passages 3 and 7 were used for the experiments. Mouse ECs from hearts, skeletal muscles, and adipose tissues were isolated as previously described (8), and efficacy was confirmed by measuring *Pecam* mRNA expression (fig. S25). Briefly, minced tissue was digested with collagenase A (2 mg/ml) with gentle agitation for 45 min at 37°C. The cell suspension was triturated, filtered through 70-μm cell strainers, and then centrifuged. Cells were resuspended in 2 ml of cold PBS with 0.1% BSA, and the cell suspension was incubated with Dynabeads (11035-mouse, Invitrogen) coated with purified antibody to CD31 (553370, BD Pharmingen) for positive selection.

Apelin-13 (Sigma-Aldrich) was used for all apelin stimulation conditions at the indicated doses and time points. For phosphorylation studies, HUVECs were serum-starved in EBM-2 with 0.2% fetal bovine serum overnight. Pretreatment with 200 nM Wortmannin (Sigma-Aldrich) or 1 μM LY-294002 (Sigma-Aldrich) was carried out for 1 hour after overnight serum starvation before apelin stimulation. Cells were washed with ice-cold PBS and lysed using radioimmunoprecipitation assay lysis buffer (Thermo Fisher Scientific) containing Halt Protease and Phosphatase Inhibitor Cocktail (Thermo Fisher Scientific). The protein concentrations were measured using the Micro BCA Protein Assay kit (Thermo Fisher Scientific). Western blotting was performed as previously described (9, 10). Each Western blot is representative of three independent experiments done in triplicates. The antibodies used were as follows: phospho-FOXO1 (Thr^{24}) (9464, Cell Signaling), FOXO1 (2880, Cell Signaling), phospho-AKT (Ser^{473}) (4060, Cell Signaling), AKT (4691, Cell Signaling), phospho-AMPKα (Thr^{172}) (2535, Cell Signaling), AMPKα (2603, Cell Signaling), phospho-eNOS (S1177) (9571, Cell Signaling), eNOS (BD 610296), glyceraldehyde-3-phosphate dehydrogenase (GAPDH) (2118, Cell Signaling), and FABP4 (AF1443, R&D Systems).

In situ hybridization

Human skeletal muscle was purchased from OriGene (CS617749). Discarded and deidentified surgical specimens of human adipose tissue were obtained from Yale New Haven Hospital. Human *APLNR* probe was made using a full-length complementary DNA (cDNA) clone (MHS6278–202801919; clone ID: 5241995, Dharmacon). Whole-mount in situ hybridization was performed as previously described (64) for human adipose tissue. Briefly, tissue was fixed in 4% paraformaldehyde (PFA) overnight at 4°C and dehydrated the next day in a methanol series. Tissue was rehydrated to PBS/0.1% Tween 20 and digested for 10 min in proteinase K (500 μg/ml) (Sigma-Aldrich), followed by fixation in 4% PFA/0.2% glutaraldehyde in PBS/0.1% Tween 20. The tissue was washed in PBS/0.1% Tween 20, preincubated in hybridization buffer for 3 hours at 70°C, and then incubated in hybridization buffer with digoxigenin (DIG)–labeled RNA probe overnight at 70°C. Section in situ hybridization was performed as previously described (65) for human skeletal muscle. Briefly, tissue was fixed in 4% PFA overnight at 4°C and then cryoprotected in 30% sucrose treated with diethyl pyrocarbonate overnight at 4°C. Tissue was frozen in OCT (optimum cutting temperature) compound (Sakura Tissue-Tek) and sectioned transversely on a Leica CM1950 cryostat at 15 to 20 μm. Sections were dried for 2 hours at room temperature and then incubated in hybridization buffer with DIG-labeled RNA probe overnight at 70°C. The probe was labeled with DIG–uridine triphosphate (11277073910, Roche) and detected with alkaline phosphatase (AP)–conjugated anti–DIG-AP antibody (11093274910, Roche) overnight at 4°C, and the signal was visualized with BM Purple AP substrate (1144207001, Roche). Adjacent skeletal muscle sections were stained with an anti-vWF antibody (A0082, Dako) overnight at 4°C and detected with Alexa Fluor 568 goat anti-rabbit IgG (A11011, Invitrogen). DAPI (Sigma-Aldrich) was used to stain the nuclei. Images were obtained using bright-field and fluorescence microscopy (PerkinElmer UltraVIEW VoX Spinning Disk and Nikon Eclipse 80i).

Intraperitoneal glucose tolerance test

Overnight-fasted mice were injected with D-glucose (2 g/kg) (D16-1, Thermo Fisher Scientific; 200 mg/ml dissolved in PBS) intraperitoneally. For analysis of blood glucose concentrations, blood was collected from the tail vein at 0, 15, 30, 60, 45, 90, and 120 min after glucose administration, and glucose was measured with a glucometer (nextEZ meter, Contour). To determine the effect of apelin on glucose tolerance, overnight-fasted $Apln r^{ECKO}$ mice were intravenously injected with apelin-13 (200 pmol/kg) (Sigma-Aldrich) or PBS 30 min before D-glucose administration. For treatment with the FABP4 inhibitor, BMS309403 (15 mg/kg per day) (60929, Astatech Inc.) was administered daily by oral gavage for 7 days.

Intraperitoneal insulin tolerance test

Mice fasted for 6 hours were injected with insulin (1 U/kg) [I9278, Sigma-Aldrich; prepared in PBS (0.1 U/ml)] intraperitoneally. For analysis of blood glucose concentrations, blood was collected from the tail vein at 0, 10, 20, 30, 40, 50, and 60 min after insulin administration, and glucose was measured with a glucometer (nextEZ meter, Contour).

BODIPY uptake and permeability assay

HUVECs or HCMECs were plated onto 24-well plates and pre-treated with 1 μM apelin for 24 hours in serum-free medium or subjected to *APLNR* knockdown for 48 hours before being incubated with 2 μM BODIPY (D3823, Life Technologies) for 90 min. Cells were washed twice with ice-cold PBS, and fluorescence was measured using a fluorescence plate reader (BioTek). To visualize the fluorescence after BODIPY uptake, the cells were fixed in 4% PFA for 10 min at room temperature and analyzed by using fluorescence microscopy (PerkinElmer UltraVIEW VoX Spinning Disk).

To evaluate the effects of apelin, APLNR, or FABP4 on FA transfer through the endothelial layer, HUVECs and HCMECs were incubated with 1 μM apelin for 24 hours or transfected with small interfering RNA (siRNA) against *APLN* and/or *APLNR*. To determine the effect of FABP4 inhibitor BMS309403 on FA uptake, cells were subjected to *APLN* and *APLNR* knockdown for 24 hours and incubated with the indicated concentrations of BMS309403 for 24 hours. Cells were then plated on Transwell inserts (0.4-μm pore size; 3413, Costar) in 24-well plates, and 2 μM BODIPY was added to the top chamber. Fluorescence was measured from the bottom chamber at the indicated time points using a fluorescence plate reader (BioTek).

Transendothelial transfer assays

HCMECs plated on 0.4–μm–pore size Transwell inserts (3413, Costar) in 24-well plates were incubated with 1 μM apelin for 2 hours before adding 100 μM 2-(*N*-(7-nitrobenz-2-oxa-1,3-diazol-4-yl)amino)-2-deoxyglucose (N13195, Thermo Fisher Scientific) or insulin-FITC (I3661, Sigma-Aldrich). Medium samples were collected from the bottom chamber at the indicated time points, and fluorescence was measured using a fluorescence plate reader (BioTek). For assessment of endothelial layer permeability, HCMECs were trans-fected with *APLN* and *APLNR* targeting siRNA (20 nM) or scramble control siRNA for 48 hours, after which the cells were plated on 0.4–μm– pore size Transwell inserts (3413, Costar) and cultured for 3 days. FITC-dextran (70 kDa) (150 μl of 1 mg/ml) was added to the upper chamber, 50 μl of medium was taken from the lower chamber at the designated time points, and fluorescence was measured using a plate reader (BioTek).

Immunohistochemistry and immunofluorescence

To assess GFP expression in the $Aplnr^{CreER}$:$Rosa^{mTmG}$ mice, mice were euthanized using CO_2 inhalation, and tissues were harvested. Tissues were fixed in 4% PFA for 1 to 2 hours at 4°C. Tissues were washed in 1× PBS and frozen in OCT (Sakura Tissue-Tek). Tissues were sectioned and immunostained with anti–VE-cadherin antibody (550548, BD Pharmingen), Sm-MHC (BT-562, Biomedical Technologies), and a nuclear stain (DAPI, Thermo Fisher Scientific) and then imaged using fluorescence microscopy.

Hearts from mice of the indicated genotype or treatment were dissected and postfixed in 4% PFA overnight and subsequently cryoprotected in 30% sucrose overnight. Tissue was then frozen in OCT compound (Sakura Tissue-Tek), sectioned on a Leica CM1950 cryostat at 10 μm, and stored at −80°C. Sections of adult mouse hearts were incubated overnight at 4°C with the indicated antibodies, including anti-FABP4 antibody (AF1443, R&D systems) and

anti-CD31 antibody (553370, BD Pharmingen), and then detected with Alexa Fluor 568 donkey anti-goat IgG (A10037, Invitrogen), Alexa Fluor 568 goat anti-rabbit IgG (A11011, Invitrogen), and/or Alexa Fluor 488 goat anti-mouse IgG antibodies (A11001, Invitrogen). DAPI (Sigma-Aldrich) was used to stain the nuclei. For cell staining, HUVECs were cultured in 35-mm glass-bottom dishes (MatTek), grown in EBM-2 overnight, and treated with 1 μM apelin for 1 hour. The cells were fixed with 4% PFA, incubated overnight at 4°C with anti-FOXO1 antibody (2880, Cell Signaling), and then detected with Alexa Fluor 568 goat anti-rabbit IgG (A11011, Invitrogen). DAPI (Sigma-Aldrich) was used to stain the nuclei. Images were obtained using fluorescence microscopy.

RNA extraction and reverse transcription PCR

We extracted total RNA with the miRNeasy RNA Isolation kit (Qiagen). Purified RNA was reverse-transcribed with the iScript cDNA Synthesis kit (Bio-Rad). Reverse transcription PCR (RT-PCR) was performed with TaqMan probes (Applied Biosystems) or SYBR Green assays (Bio-Rad) on a CFX96 (Bio-Rad) PCR machine according to the manufacturer's instructions.

RNA silencing

Targeting siRNAs and nontargeting controls were purchased from Invitrogen (Stealth siRNA). SiRNAs were complexed with Lipofectamine RNAiMAX (Invitrogen), and transfection was performed according to the manufacturer's instructions. Three days after the transfection, either HUVECs or HCMECs were used for the Western blot assays or real-time PCR. Efficiency of knockdown was confirmed by RT-PCR for *APLN* and *PPARG* (fig. S26) and by Western blot for APLNR (fig. S27).

LacZ staining

Apln$^{+/lacz}$ reporter mice were dissected in PBS/2 mM $MgCl_2$, and tissues were fixed in 1% PFA/0.2% glutaraldehyde for 1 hour, washed extensively, and stained in X-gal substrate solution for 24 hours at 37°C. Tissues were postfixed in 4% PFA for 1 hour at room temperature, washed, and cryoprotected in 30% sucrose/PBS. Tissues were subsequently frozen in OCT (Sakura Tissue-Tek), sectioned at 20 μm, washed with PBS to remove the OCT, and mounted with DPX mounting medium (Sigma-Aldrich).

In vivo FA uptake assay

Eight- to 12-week-old male mice were given a bolus dose of 2 μCi of ^{14}C-OA (PerkinElmer) dissolved in olive oil by oral gavage. For treatment with the FABP4 inhibitor, BMS309403 (15 mg/kg per day) (60929, Astatech Inc.) was administered daily by oral gavage for 7 days. For analysis of FA uptake, organs were harvested at the indicated time points after ^{14}C-OA gavage. The organs were dissolved overnight at 50°C in tissue solubilizer (1 ml/100 mg tissue) and neutralized with glacial acetic acid (30 μl/ml), and BCS-NA Counting Scintillant was added. Total radioactivity was measured by liquid scintillation using a Tri-Carb 1600TR Liquid Scintillator (Packard).

Oil red O staining

Frozen 10-μm cryosections from the heart and skeletal muscle were fixed with 10% neutral buffered formalin for 5 min. After the fixation, oil red O stain (O1391, Sigma-Aldrich) was added for 10 min to stain for lipid accumulation. After rinsing with distilled water, the slides were mounted with aqueous VectaMount AQ (H-5501, Vector Laboratories) solution. Sections were imaged using bright-field microscopy and quantified using ImageJ.

Tissue lipid analysis

Lipids were extracted using the method of Folch *et al.* (66). The extracts were filtered, and lipids were recovered in the chloroform phase. Individual lipid classes were separated by thin-layer chromatography using Silica Gel 60 A plates developed in petroleum ether, ethyl ether, and acetic acid (80:20:1) and visualized by rhodamine 6G. Phospholipids, diglycerides, triglycerides, and cholesteryl esters were scraped from the plates and methylated using BF3/methanol, as described (67). The methylated FAs were extracted and analyzed by gas chromatography. Gas chromatography analyses were carried out on an HP 5890 gas chromatograph equipped with flame ionization detectors, an Agilent 7890A GC system, and a capillary column (0.25 mm × 30 m, 0.25-μm film; SP-2380, Supelco). Helium was used as a carrier gas. The oven temperature was programmed to increase from 160° to 230°C at increments of 4°C/min. FA methyl esters were identified by comparing the retention times to those of known standards. Inclusion of lipid standards with odd-chain FAs permitted quantitation of the amount of lipid in the sample. Dipentadecanoyl phosphatidylcholine (C15:0), diheptadecanoin (C17:0), trieicosenoin (C20:1), and cholesteryl eicosenoate (C20:1) were used as standards.

Microarray

HUVECs were transfected with *APLN*, *APLNR*, *FOXO1*, or negative control siRNAs (Invitrogen). After 48 hours, RNA was extracted using miRNeasy Mini kit (Qiagen). The RNA was quantified, and the RNA quality was verified using NanoDrop (Thermo Fisher Scientific). The HumanHT-12 v4 Expression BeadChip kit (Illumina) was used according to the manufacturer's protocol by the Yale Center for Genome Analysis. Microarray results were analyzed using the bead array and limma packages in R/Bioconductor (version 2.14/2.09). The gene expression profiling data have been deposited into GEO (GSE67390).

Plasma analysis

Plasma was assessed for insulin (10-1247-01, Mercodia) and adiponec-tin (EK0596, BOSTER), following the manufacturer's instructions. Briefly, for insulin, 10 μl of each plasma sample was added in the insulin antibody–coated wells on the microplate. After a 2-hour incubation, the plate was washed, and the substrate was added at room temperature. The reaction was stopped after 15 min, and the plate was read at 450 nm (BioTek Synergy 2). For adiponectin, 100 μl of plasma was added to adiponectin antibody–coated wells on the microplate and incubated for 2 hours at 37°C. The plate was washed, and substrates were added, followed by an additional 1-hour incubation, after which the stop solution was added and the absorption at 450 nm was measured with a microplate reader.

Statistics

All experiments were performed in triplicate (unless otherwise specified) in at least three independent experiments, and data are shown as means ± SEM. When only two groups were compared, statistical differences were assessed with unpaired two-tailed Student's *t* test. Otherwise, statistical significance was determined using one- or two-way analysis of variance, followed by Bonferroni multiple comparison test. $P < 0.05$ was considered statistically significant.

Supplementary Material

Refer to Web version on PubMed Central for supplementary material.

Acknowledgments

We thank R. Adams for providing the Cdh5(PAC)-CreERT2 mice; G. Zarkada for the assistance with the in vivo studies; J. P. Camporez, R. Perry, and A. Nasiri of the Yale Mouse Metabolic Phenotyping Center for the body composition analysis; E. Brittain and C. Harris of the Vanderbilt Mouse Metabolic Phenotyping Center and W. Zavadoski of Vascumab LLC for the tissue FA/triglyceride analyses; D. Defilippo for the administrative assistance; and R. Webber, N. Copeland, and W. Evangelisti for the assistance with mouse colonies.

Funding: This work was supported by grants from the NIH (HL095654, HL113005, and HL101284 to H.J.C; AI102888 and CA008748 to M.O.L.; GM103652 to A.R.M.; HL135767 to A.M.; HL128503 to K.R.-H.; DK59637 to the Vanderbilt Mouse Metabolic Phenotyping Center), the Howard Hughes Medical Institute (Physician Scientist Early Career Award to H.J.C. and Faculty Scholar Award to M.O.L.), the American Diabetes Association (Basic Science grant 1-14-BS-035 to H.J.C.), the American Heart Association (Established Investigator Award to H.J.C.), and the U.S. Department of Veteran Affairs (7IK2BX002527 to A.R.M.) and by the Actelion Entelligence Award (to A.R.M.)

REFERENCES AND NOTES

1. Aird WC. Phenotypic heterogeneity of the endothelium: II. Representative vascular beds. Circ. Res. 2007; 100:174–190. [PubMed: 17272819]
2. Aird WC. Phenotypic heterogeneity of the endothelium: I. Structure, function, and mechanisms. Circ. Res. 2007; 100:158–173. [PubMed: 17272818]
3. Unger RH. Lipotoxic diseases. Annu. Rev. Med. 2002; 53:319–336. [PubMed: 11818477]
4. Samuel VT, Petersen KF, Shulman GI. Lipid-induced insulin resistance: Unravelling the mechanism. Lancet. 2010; 375:2267–2277. [PubMed: 20609972]
5. Roden M, Price TB, Perseghin G, Petersen KF, Rothman DL, Cline GW, Shulman GI. Mechanism of free fatty acid-induced insulin resistance in humans. J. Clin. Invest. 1996; 97:2859–2865. [PubMed: 8675698]
6. Perseghin G, Scifo P, De Cobelli F, Pagliato E, Battezzati A, Arcelloni C, Vanzulli A, Testolin G, Pozza G, Del Maschio A, Luzi L. Intramyocellular triglyceride content is a determinant of in vivo insulin resistance in humans: A 1H-13C nuclear magnetic resonance spectroscopy assessment in offspring of type 2 diabetic parents. Diabetes. 1999; 48:1600–1606. [PubMed: 10426379]
7. Shulman GI. Ectopic fat in insulin resistance, dyslipidemia, and cardiometabolic disease. N. Engl. J. Med. 2014; 371:1131–1141. [PubMed: 25229917]
8. Kang Y, Kim J, Anderson JP, Wu J, Gleim SR, Kundu RK, McLean DL, Kim J-d, Park H, Jin S-w, Hwa J, Quertermous T, Chun HJ. Apelin-APJ signaling is a critical regulator of endothelial MEF2 activation in cardiovascular development. Circ. Res. 2013; 113:22–31. [PubMed: 23603510]
9. Chandra SM, Razavi H, Kim J, Agrawal R, Kundu RK, de Jesus Perez V, Zamanian RT, Quertermous T, Chun HJ. Disruption of the apelin-APJ system worsens hypoxiainduced pulmonary hypertension. Arterioscler. Thromb. Vasc. Biol. 2011; 31:814–820. [PubMed: 21233449]
10. Chun HJ, Ali ZA, Kojima Y, Kundu RK, Sheikh AY, Agrawal R, Zheng L, Leeper NJ, Pearl NE, Patterson AJ, Anderson JP, Tsao PS, Lenardo MJ, Ashley EA, Quertermous T. Apelin signaling

antagonizes Ang II effects in mouse models of atherosclerosis. J. Clin. Invest. 2008; 118:3343–3354. [PubMed: 18769630]

11. McLean DL, Kim J, Kang Y, Shi H, Atkins GB, Jain MK, Chun HJ. Apelin/APJ signaling is a critical regulator of statin effects in vascular endothelial cells—Brief report. Arterioscler. Thromb. Vasc. Biol. 2012; 32:2640–2643. [PubMed: 22995518]
12. Dray C, Knauf C, Daviaud D, Waget A, Boucher J, Buléon M, Cani PD, Attane C, Guigné C, Carpéné C, Burcelin R, Castan-Laurell I, Valet P. Apelin stimulates glucose utilization in normal and obese insulin-resistant mice. Cell Metab. 2008; 8:437–445. [PubMed: 19046574]
13. Yue P, Jin H, Aillaud M, Deng AC, Azuma J, Asagami T, Kundu RK, Reaven GM, Quertermous T, Tsao PS. Apelin is necessary for the maintenance of insulin sensitivity. Am. J. Physiol. Endocrinol. Metab. 2010; 298:E59–E67. [PubMed: 19861585]
14. Zoungas S, Chalmers J, Neal B, Billot L, Li Q, Hirakawa Y, Arima H, Monaghan H, Joshi R, Colagiuri S, Cooper ME, Glasziou P, Grobbee D, Hamet P, Harrap S, Heller S, Lisheng L, Mancia G, Marre M, Matthews DR, Mogensen CE, Perkovic V, Poulter N, Rodgers A, Williams B, MacMahon S, Patel A, Woodward M. ADVANCE-ON Collaborative Group. Follow-up of blood-pressure lowering and glucose control in type 2 diabetes. N. Engl. J. Med. 2014; 371:1392–1406. [PubMed: 25234206]
15. ADVANCE Collaborative Group. Intensive blood glucose control and vascular outcomes in patients with type 2 diabetes. N. Engl. J. Med. 2008; 358:2560–2572. [PubMed: 18539916]
16. Action to Control Cardiovascular Risk in Diabetes Study Group. Effects of intensive glucose lowering in type 2 diabetes. N. Engl. J. Med. 2008; 358:2545–2559. [PubMed: 18539917]
17. Neal B, Perkovic V, de Zeeuw D, Mahaffey KW, Fulcher G, Stein P, Desai M, Shaw W, Jiang J, Vercruysse F, Meininger G, Matthews D. Rationale, design, and baseline characteristics of the Canagliflozin Cardiovascular Assessment Study (CANVAS)—A randomized placebo-controlled trial. Am. Heart J. 2013; 166:217–223. e211. [PubMed: 23895803]
18. White WB, Cannon CP, Heller SR, Nissen SE, Bergenstal RM, Bakris GL, Perez AT, Fleck PR, Mehta CR, Kupfer S, Wilson C, Cushman WC, Zannad F. EXAMINE Investigators, Alogliptin after acute coronary syndrome in patients with type 2 diabetes. N. Engl. J. Med. 2013; 369:1327–1335. [PubMed: 23992602]
19. Scirica BM, Bhatt DL, Braunwald E, Steg PG, Davidson J, Hirshberg B, Ohman P, Frederich R, Wiviott SD, Hoffman EB, Cavender MA, Udell JA, Desai NR, Mosenzon O, McGuire DK, Ray KK, Leiter LA, Raz I. SAVOR-TIMI 53 Steering Committee and Investigators, Saxagliptin and cardiovascular outcomes in patients with type 2 diabetes mellitus. N. Engl. J. Med. 2013; 369:1317–1326. [PubMed: 23992601]
20. Chen HI, Sharma B, Akerberg BN, Numi HJ, Kivelä R, Saharinen P, Aghajanian H, McKay AS, Bogard PE, Chang AH, Jacobs AH, Epstein JA, Stankunas K, Alitalo K, Red-Horse K. The sinus venosus contributes to coronary vasculature through VEGFC-stimulated angiogenesis. Development. 2014; 141:4500–4512. [PubMed: 25377552]
21. Muzumdar MD, Tasic B, Miyamichi K, Li L, Luo L. A global double-fluorescent Cre reporter mouse. Genesis. 2007; 45:593–605. [PubMed: 17868096]
22. Charo DN, Ho M, Fajardo G, Kawana M, Kundu RK, Sheikh AY, Finsterbach TP, Leeper NJ, Ernst KV, Chen MM, Ho YD, Chun HJ, Bernstein D, Ashley EA, Quertermous T. Endogenous regulation of cardiovascular function by apelin-APJ. Am. J. Physiol. Heart Circ. Physiol. 2009; 297:H1904–H1913. [PubMed: 19767528]
23. Benedito R, Roca C, Sörensen I, Adams S, Gossler A, Fruttiger M, Adams RH. The notch ligands Dll4 and Jagged1 have opposing effects on angiogenesis. Cell. 2009; 137:1124–1135. [PubMed: 19524514]
24. Sheikh AY, Chun HJ, Glassford AJ, Kundu RK, Kutschka I, Ardigo D, Hendry SL, Wagner RA, Chen MM, Ali ZA, Yue P, Huynh DT, Connolly AJ, Pelletier MP, Tsao PS, Robbins RC, Quertermous T. In vivo genetic profiling and cellular localization of apelin reveals a hypoxia-sensitive, endothelial-centered pathway activated in ischemic heart failure. Am. J. Physiol. Heart Circ. Physiol. 2008; 294:H88–H98. [PubMed: 17906101]
25. Brunet A, Bonni A, Zigmond MJ, Lin MZ, Juo P, Hu LS, Anderson MJ, Arden KC, Blenis J, Greenberg ME. Akt promotes cell survival by phosphorylating and inhibiting a Forkhead transcription factor. Cell. 1999; 96:857–868. [PubMed: 10102273]

26. Medema RH, Kops GJPL, Bos JL, Burgering BMT. AFX-like Forkhead transcription factors mediate cell-cycle regulation by Ras and PKB through $p27^{kip1}$. Nature. 2000; 404:782–787. [PubMed: 10783894]
27. Accili D, Arden KC. FoxOs at the crossroads of cellular metabolism, differentiation, and transformation. Cell. 2004; 117:421–426. [PubMed: 15137936]
28. Potente M, Urbich C, Sasaki K-i, Hofmann WK, Heeschen C, Aicher A, Kollipara R, DePinho RA, Zeiher AM, Dimmeler S. Involvement of Foxo transcription factors in angiogenesis and postnatal neovascularization. J. Clin. Invest. 2005; 115:2382–2392. [PubMed: 16100571]
29. Shin D, Anderson DJ. Isolation of arterial-specific genes by subtractive hybridization reveals molecular heterogeneity among arterial endothelial cells. Dev. Dyn. 2005; 233:1589–1604. [PubMed: 15977181]
30. Aragonès G, Saavedra P, Heras M, Cabrè A, Girona J, Masana L. Fatty acid-binding protein 4 impairs the insulin-dependent nitric oxide pathway in vascular endothelial cells. Cardiovasc. Diabetol. 2012; 11:72.
31. Spiegelman BM, Green H. Control of specific protein biosynthesis during the adipose conversion of 3T3 cells. J. Biol. Chem. 1980; 255:8811–8818. [PubMed: 6773950]
32. Tontonoz P, Hu E, Graves RA, Budavari AI, Spiegelman BM. mPPARg2: Tissue-specific regulator of an adipocyte enhancer. Genes Dev. 1994; 8:1224–1234. [PubMed: 7926726]
33. Ouyang W, Beckett O, Flavell RA, Li MO. An essential role of the Forkhead-box transcription factor Foxo1 in control of T cell homeostasis and tolerance. Immunity. 2009; 30:358–371. [PubMed: 19285438]
34. Van der Vusse GJ, Glatz JF, Van Nieuwenhoven FA, Reneman RS, Bassingthwaighte JB. Transport of long-chain fatty acids across the muscular endothelium. Adv. Exp. Med. Biol. 1998; 441:181–191. [PubMed: 9781325]
35. Sulsky R, Magnin DR, Huang Y, Simpkins L, Taunk P, Patel M, Zhu Y, Stouch TR, Bassolino-Klimas D, Parker R, Harrity T, Stoffel R, Taylor DS, Lavoie TB, Kish K, Jacobson BL, Sheriff S, Adam LP, Ewing WR, Robl JA. Potent and selective biphenyl azole inhibitors of adipocyte fatty acid binding protein (aFABP). Bioorg. Med. Chem. Lett. 2007; 17:3511–3515. [PubMed: 17502136]
36. Furuhashi M, Tuncman G, Görgün CZ, Makowski L, Atsumi G, Vaillancourt E, Kono K, Babaev VR, Fazio S, Linton MF, Sulsky R, Robl JA, Parker RA, Hotamisligil GS. Treatment of diabetes and atherosclerosis by inhibiting fatty-acid-binding protein aP2. Nature. 2007; 447:959–965. [PubMed: 17554340]
37. Sawane M, Kajiya K, Kidoya H, Takagi M, Muramatsu F, Takakura N. Apelin inhibits diet-induced obesity by enhancing lymphatic and blood vessel integrity. Diabetes. 2013; 62:1970–1980. [PubMed: 23378608]
38. Hagberg CE, Falkevall A, Wang X, Larsson E, Huusko J, Nilsson I, van Meeteren LA, Samen E, Lu L, Vanwildemeersch M, Klar J, Genove G, Pietras K, Stone-Elander S, Claesson-Welsh L, Ylä-Herttuala S, Lindahl P, Eriksson U. Vascular endothelial growth factor B controls endothelial fatty acid uptake. Nature. 2010; 464:917–921. [PubMed: 20228789]
39. Hagberg CE, Mehlem A, Falkevall A, Muhl L, Fam BC, Ortsäter H, Scotney P, Nyqvist D, Samén E, Lu L, Stone-Elander S, Proietto J, Andrikopoulos S, Sjöholm A, Nash A, Eriksson U. Targeting VEGF-B as a novel treatment for insulin resistance and type 2 diabetes. Nature. 2012; 490:426–430. [PubMed: 23023133]
40. Kanda T, Brown JD, Orasanu G, Vogel S, Gonzalez FJ, Sartoretto J, Michel T, Plutzky J. PPARg in the endothelium regulates metabolic responses to high-fat diet in mice. J. Clin. Invest. 2009; 119:110–124. [PubMed: 19065047]
41. Jang C, Oh SF, Wada S, Rowe GC, Liu L, Chan MC, Rhee J, Hoshino A, Kim B, Ibrahim A, Baca LG, Kim E, Ghosh CC, Parikh SM, Jiang A, Chu Q, Forman DE, Lecker SH, Krishnaiah S, Rabinowitz JD, Weljie AM, Baur JA, Kasper DL, Arany Z. A branched-chain amino acid metabolite drives vascular fatty acid transport and causes insulin resistance. Nat. Med. 2016; 22:421–426. [PubMed: 26950361]

42. Yang P, Maguire JJ, Davenport AP. Apelin, Elabela/Toddler, and biased agonists as novel therapeutic agents in the cardiovascular system. Trends Pharmacol. Sci. 2015; 36:560–567. [PubMed: 26143239]
43. Boucher J, Masri B, Daviaud D, Gesta S, Guigné C, Mazzucotelli A, Castan-Laurell I, Tack I, Knibiehler B, Carpéné C, Audigier Y, Saulnier-Blache J-S, Valet P. Apelin, a newly identified adipokine up-regulated by insulin and obesity. Endocrinology. 2005; 146:1764–1771. [PubMed: 15677759]
44. Erdem G, Dogru T, Tasci I, Sonmez A, Tapan S. Low plasma apelin levels in newly diagnosed type 2 diabetes mellitus. Exp. Clin. Endocrinol. Diabetes. 2008; 116:289–292. [PubMed: 18484561]
45. Li L, Yang G, Li Q, Tang Y, Yang M, Yang H, Li K. Changes and relations of circulating visfatin, apelin, and resistin levels in normal, impaired glucose tolerance, and type 2 diabetic subjects. Exp. Clin. Endocrinol. Diabetes. 2006; 114:544–548. [PubMed: 17177135]
46. Japp AG, Cruden NL, Barnes G, van Gemeren N, Mathews J, Adamson J, Johnston NR, Denvir MA, Megson IL, Flapan AD, Newby DE. Acute cardiovascular effects of apelin in humans: Potential role in patients with chronic heart failure. Circulation. 2010; 121:1818–1827. [PubMed: 20385929]
47. Japp AG, Cruden NL, Amer DA, Li VKY, Goudie EB, Johnston NR, Sharma S, Neilson I, Webb DJ, Megson IL, Flapan AD, Newby DE. Vascular effects of apelin in vivo in man. J. Am. Coll. Cardiol. 2008; 52:908–913. [PubMed: 18772060]
48. Bertero T, Lu Y, Annis S, Hale A, Bhat B, Saggar R, Saggar R, Wallace WD, Ross DJ, Vargas SO, Graham BB, Kumar R, Black SM, Fratz S, Fineman JR, West JD, Haley KJ, Waxman AB, Chau BN, Cottrill KA, Chan SY. Systems-level regulation of microRNA networks by miR-130/301 promotes pulmonary hypertension. J. Clin. Invest. 2014; 124:3514–3528. [PubMed: 24960162]
49. Alastalo T-P, Li M, Perez Vde J, Pham D, Sawada H, Wang JK, Koskenvuo M, Wang L, Freeman BA, Chang HY, Rabinovitch M. Disruption of PPARg/b-catenin-mediated regulation of apelin impairs BMP-induced mouse and human pulmonary arterial EC survival. J. Clin. Invest. 2011; 121:3735–3746. [PubMed: 21821917]
50. Tanaka J, Qiang L, Banks AS, Welch CL, Matsumoto M, Kitamura T, Ido-Kitamura Y, DePinho RA, Accili D. Foxo1 links hyperglycemia to LDL oxidation and endothelial nitric oxide synthase dysfunction in vascular endothelial cells. Diabetes. 2009; 58:2344–2354. [PubMed: 19584310]
51. Sengupta A, Chakraborty S, Paik J, Yutzey KE, Evans-Anderson HJ. FoxO1 is required in endothelial but not myocardial cell lineages during cardiovascular development. Dev. Dyn. 2012; 241:803–813. [PubMed: 22411556]
52. Tsuchiya K, Tanaka J, Shuiqing Y, Welch CL, DePinho RA, Tabas I, Tall AR, Goldberg IJ, Accili D. FoxOs integrate pleiotropic actions of insulin in vascular endothelium to protect mice from atherosclerosis. Cell Metab. 2012; 15:372–381. [PubMed: 22405072]
53. Furuyama T, Kitayama K, Shimoda Y, Ogawa M, Sone K, Yoshida-Araki K, Hisatsune H, Nishikawa S-i, Nakayama K, Nakayama K, Ikeda K, Motoyama N, Mori N. Abnormal angiogenesis in Foxo1 (Fkhr)-deficient mice. J. Biol. Chem. 2004; 279:34741–34749. [PubMed: 15184386]
54. Nakae J, Park B-C, Accili D. Insulin stimulates phosphorylation of the forkhead transcription factor FKHR on serine 253 through a Wortmannin-sensitive pathway. J. Biol. Chem. 1999; 274:15982–15985. [PubMed: 10347145]
55. Kearney MT. Changing the way we think about endothelial cell insulin sensitivity, nitric oxide, and the pathophysiology of type 2 diabetes: The FoxO is loose. Diabetes. 2013; 62:1386–1388. [PubMed: 23613560]
56. Tsuchiya K, Accili D. Liver sinusoidal endothelial cells link hyperinsulinemia to hepatic insulin resistance. Diabetes. 2013; 62:1478–1489. [PubMed: 23349480]
57. Attané C, Foussal C, Le Gonidec S, Benani A, Daviaud D, Wanecq E, Guzmán-Ruiz R, Dray C, Bezaire V, Rancoule C, Kuba K, Ruiz-Gayo M, Levade T, Penninger J, Burcelin R, Pénicaud L, Valet P, Castan-Laurell I. Apelin treatment increases complete fatty acid oxidation, mitochondrial oxidative capacity, and biogenesis in muscle of insulin-resistant mice. Diabetes. 2012; 61:310–320. [PubMed: 22210322]

58. Greer EL, Oskoui PR, Banko MR, Maniar JM, Gygi MP, Gygi SP, Brunet A. The energy sensor AMP-activated protein kinase directly regulates the mammalian FOXO3 transcription factor. J. Biol. Chem. 2007; 282:30107–30119. [PubMed: 17711846]

59. Elmasri H, Karaaslan C, Teper Y, Ghelfi E, Weng M, Ince TA, Kozakewich H, Bischoff J, Cataltepe S. Fatty acid binding protein 4 is a target of VEGF and a regulator of cell proliferation in endothelial cells. FASEB J. 2009; 23:3865–3873. [PubMed: 19625659]

60. Lee MYK, Li HY, Xiao Y, Zhou ZG, Xu AM, Vanhoutte PM. Chronic administration of BMS309403 improves endothelial function in apolipoprotein E-deficient mice and in cultured human endothelial cells. Br. J. Pharmacol. 2011; 162:1564–1576. [PubMed: 21175571]

61. Lan H, Cheng C-C, Kowalski TJ, Pang L, Shan L, Chuang CC, Jackson J, Rojas-Triana A, Bober L, Liu L, Voigt J, Orth P, Yang X, Shipps GW Jr, Hedrick JA. Small-molecule inhibitors of FABP4/5 ameliorate dyslipidemia but not insulin resistance in mice with diet-induced obesity. J. Lipid Res. 2011; 52:646–656. [PubMed: 21296956]

62. Maeda K, Cao H, Kono K, Gorgun CZ, Furuhashi M, Uysal KT, Cao Q, Atsumi G, Malone H, Krishnan B, Minokoshi Y, Kahn BB, Parker RA, Hotamisligil GS. Adipocyte/ macrophage fatty acid binding proteins control integrated metabolic responses in obesity and diabetes. Cell Metab. 2005; 1:107–119. [PubMed: 16054052]

63. Radu M, Chernoff J. An in vivo assay to test blood vessel permeability. J. Vis. Exp. 2013; 2013:e50062.

64. Wilkinson, DG. Situ Hybridization: A Practical Approach. Oxford University Press; 1992.

65. Faux C, Rakic S, Andrews W, Yanagawa Y, Obata K, Parnavelas JG. Differential gene expression in migrating cortical interneurons during mouse forebrain development. J. Comp. Neurol. 2010; 518:1232–1248. [PubMed: 20151419]

66. Folch J, Lees M, Sloane Stanley GH. A simple method for the isolation and purification of total lipides from animal tissues. J. Biol. Chem. 1957; 226:497–509. [PubMed: 13428781]

67. Morrison WR, Smith LM. Preparation of fatty acid methyl esters and dimethylacetals from lipids with boron fluoride-methanol. J. Lipid Res. 1964; 5:600–608. [PubMed: 14221106]

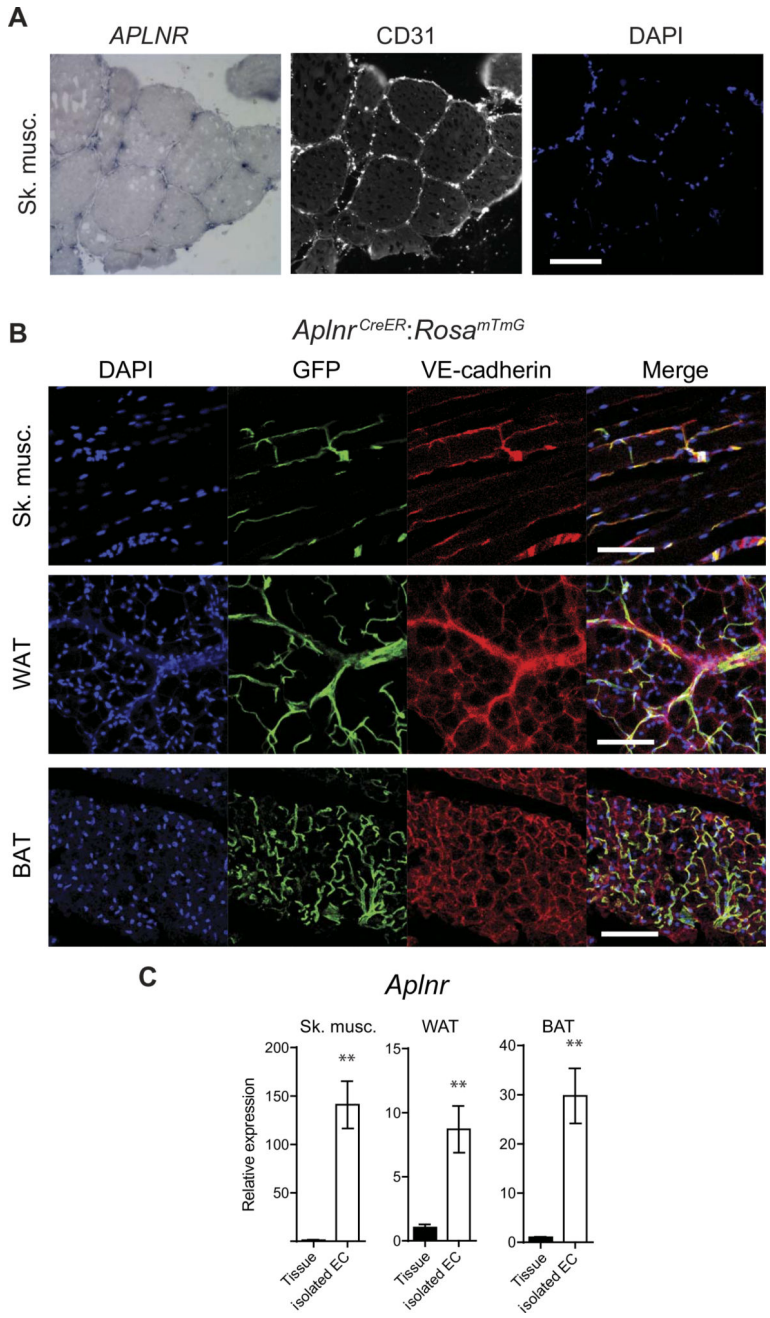

Fig. 1. APLNR expression is restricted to the endothelium of adult tissues

(**A**) Representative in situ hybridization of adult human skeletal muscle with adjacent sections stained for von Willebrand factor (vWF) (white) and with 4′,6-diamidino-2-phenylindole (DAPI) (blue). Scale bar, 50 μm. (**B**) Representative green fluorescent protein (GFP) expression in the tissues of adult *Aplnr*^{CreER}:*Rosa*^{mTmG} mice. DAPI nuclear stain (blue), GFP expression (green), VE-cadherin endothelial stain (red), and merged images are shown for skeletal muscle (Sk. musc.), WAT, and BAT. Scale bars, 100 μm. (**C**) Relative mRNA expression of *Aplnr* in tissue homogenates versus isolated ECs from various mouse adult tissues ($n = 3$ mice per group). $^{**}P < 0.01$.

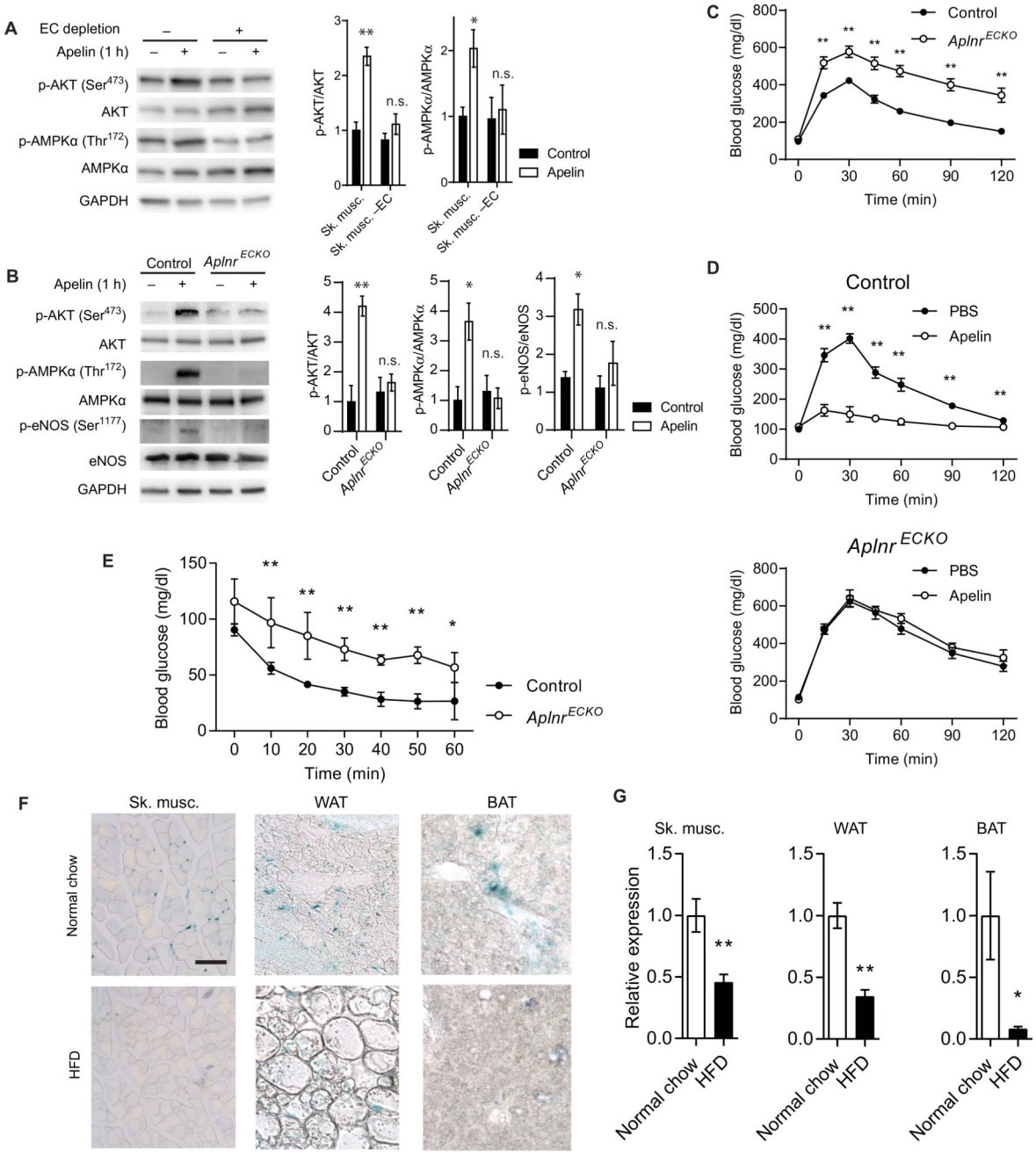

Fig. 2. Endothelial APLNR is critical for apelin signaling

(**A**) Representative immunoblot of AKT and AMPKα phosphorylation in response to apelin stimulation in skeletal muscle with or without EC depletion ($n = 3$ replicates per group). GAPDH, glyceraldehyde-3-phosphate dehydrogenase; n.s., not significant. (**B**) Representative immunoblot of AKT, AMPKα, and eNOS phosphorylation in response to apelin stimulation in skeletal muscle of *Aplnr*^{ECKO} mice and control littermates ($n = 3$ replicates per group). (**C**) IPGTT of *Aplnr*^{ECKO} mice and control littermates [$n = 10$ (control) and 14 (*Aplnr*^{ECKO})]. (**D**) IPGTT in *Aplnr*^{ECKO} and control mice 30 min after intravenous apelin injection [$n = 5$ (control) and 7 (*Aplnr*^{ECKO})]. (**E**) Intraperitoneal insulin

tolerance testing of $Apln^{ECKO}$ mice and their control littermates under basal conditions (n = 6 per group). (**F**) Representative apelin expression in skeletal muscle, WAT, and BAT, as assessed by lacZ staining of $Apln^{+/lacz}$ reporter mice fed a normal chow or a high-fat diet (HFD). Scale bar, 100 μm. (**G**) Relative mRNA expression of apelin in various tissues of mice fed a normal chow or a high-fat diet (n = 5 per group). *P < 0.05 and **P < 0.01.

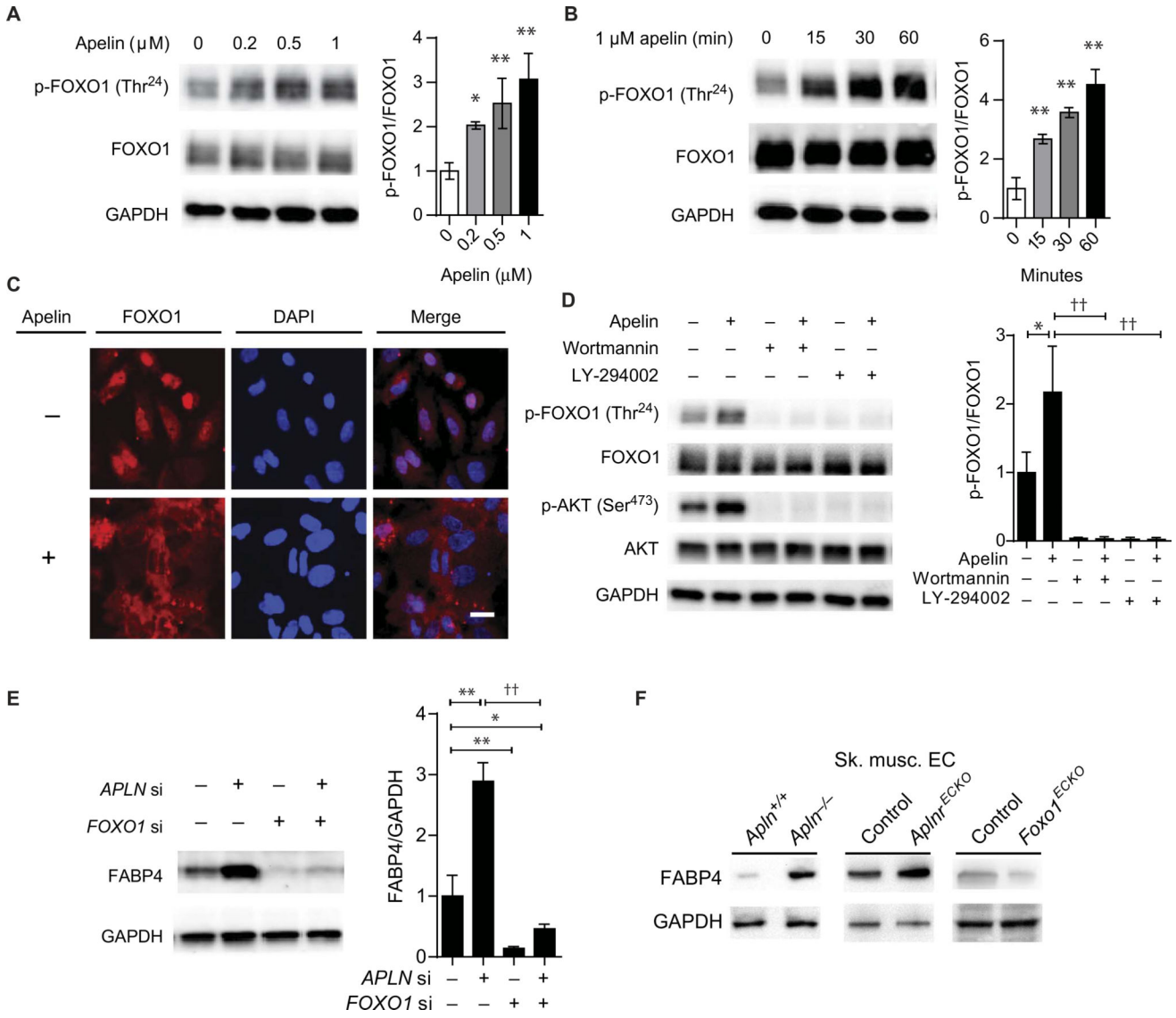

Fig. 3. Apelin induces endothelial FOXO1 inactivation and inhibits FABP4 expression

(**A**) FOXO1 phosphorylation in response to apelin stimulation (1 hour at the indicated concentrations) of HUVECs. (**B**) Time course of FOXO1 phosphorylation in HUVECs treated with apelin. (**C**) Subcellular localization of FOXO1 in response to apelin stimulation. Scale bar, 5 μm. (**D**) Apelin-induced FOXO1 phosphorylation in conjunction with inhibition of phosphoinositide 3-kinase by pretreatment with either Wortmannin or LY-294002. (**E**) Representative immunoblot of FABP4 in HUVECs in response to apelin knockdown (*APLN* si), *FOXO1* knockdown (*FOXO1* si), or both. (**F**) Representative immunoblot for FABP4 expression in isolated skeletal muscle ECs from the indicated mouse strains. $*P < 0.05$, $**P < 0.01$, and $^{\dagger\dagger}P < 0.01$.

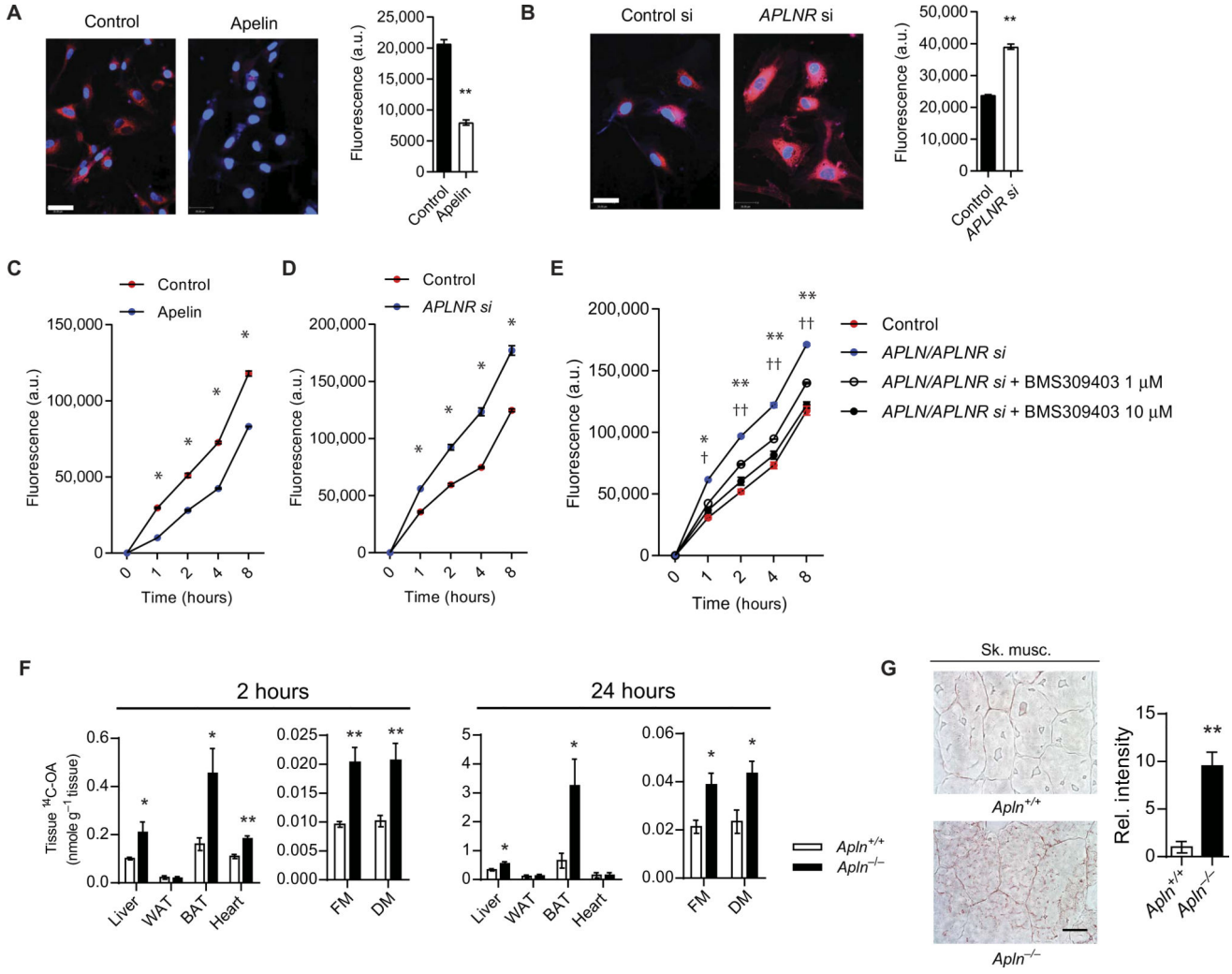

Fig. 4. Apelin-FABP4 signaling regulates endothelial FA uptake and transfer

(**A**) Representative image of BODIPY uptake in HCMECs subjected to apelin pretreatment. Scale bar, 5 μm. a.u., arbitrary units. (**B**) Representative image of BODIPY uptake in HCMECs subjected to *APLNR* knockdown (*APLNR* si). Scale bar, 5 μm. (**C** and **D**) Assessment of the FA transfer across a confluent HCMEC layer, as measured by determination of BODIPY in the bottom well of a Transwell plate, in response to apelin stimulation (C) or *APLNR* knockdown (D). (**E**) Fluorescent BODIPY transfer in response to *APLN* and *APLNR* knockdown in HCMECs and in conjunction with treatment with the FABP4 inhibitor BMS309403. $*P < 0.05$ and $**P < 0.01$ (for 1 μM); $^{\dagger}P < 0.05$ and $^{\dagger\dagger}P < 0.01$ (for 10 μM). (**F**) Tissue uptake of ^{14}C-OA in the liver, WAT, BAT, heart, and skeletal muscle of $Apln^{-/-}$ mice at 2 and 24 hours after oral gavage ($n = 5$ for each time point). FM, femoral muscle; DM, dorsi muscle. (**G**) Representative images and quantification of oil red O staining of skeletal muscle from $Apln^{-/-}$ mice and wild-type littermates ($n = 5$ per group). Scale bar, 20 μm.

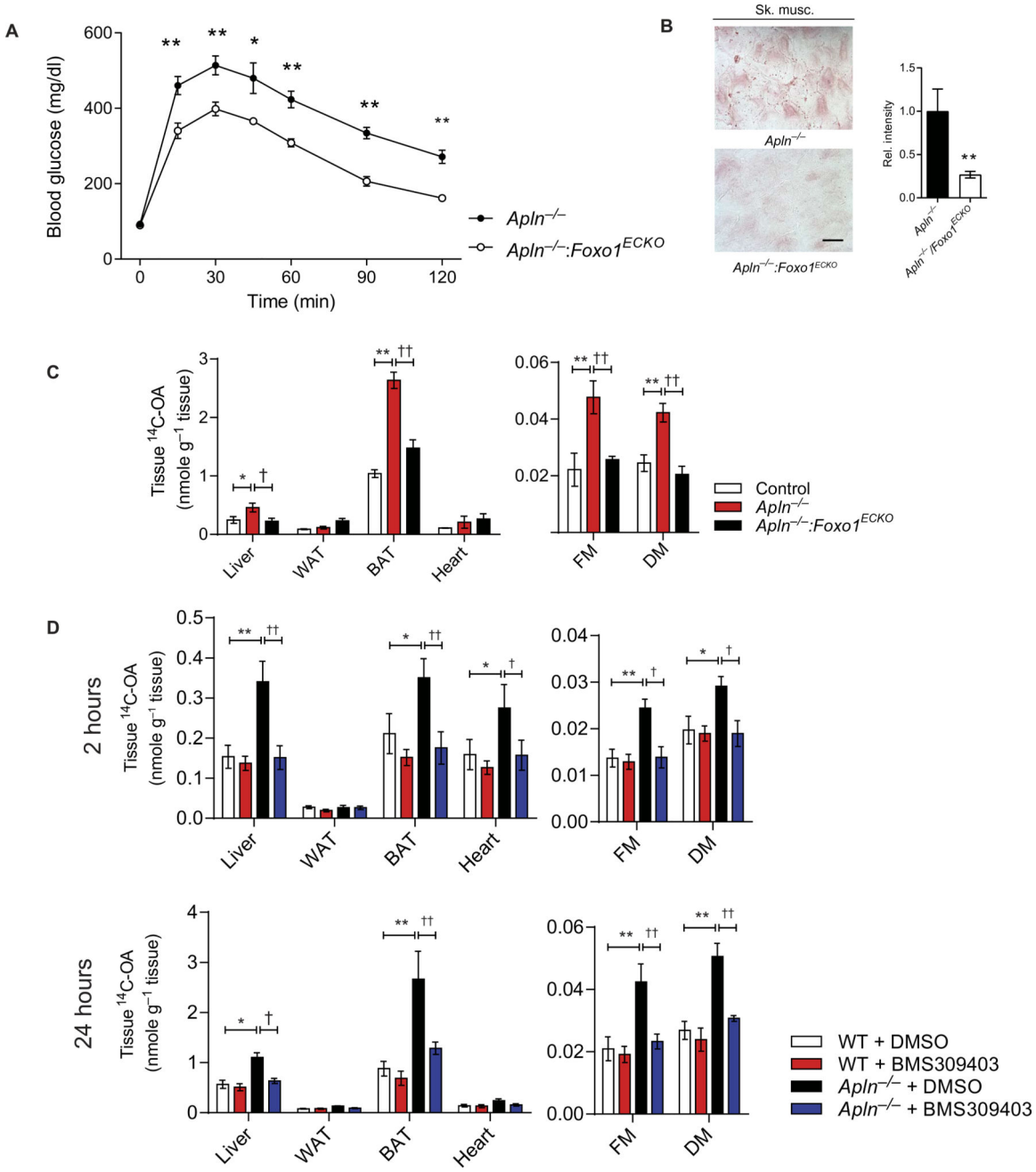

Fig. 5. Apelin-FOXO1 signaling regulates tissue FA uptake in vivo

(**A**) IPGTT in *Apln*$^{-/-}$ and *Apln*$^{-/-}$*Foxo1*^{ECKO} double-knockout mice ($n = 5$ per group). (**B**) Representative images and quantification of oil red O staining of skeletal muscle from *Apln*$^{-/-}$ and *Apln*$^{-/-}$*Foxo1*^{ECKO} double-knockout mice ($n = 5$ per group). Scale bar, 20 μm. (**C**) Assessment of ^{14}C-OA uptake in *Apln*$^{-/-}$ and *Apln*$^{-/-}$*Foxo1*^{ECKO} double-knockout mice at 24 hours after oral gavage ($n = 5$ per group). (**D**) Assessment of ^{14}C-OA uptake in *Apln*$^{-/-}$ mice and wild-type (WT) littermates treated with the FABP4 inhibitor BMS309403 ($n = 5$ per group for each time point). DMSO, dimethyl sulfoxide. Data are means ± SEM. *$P < 0.05$, **$P < 0.01$, $^{\dagger}P < 0.05$, and $^{\dagger\dagger}P < 0.01$.

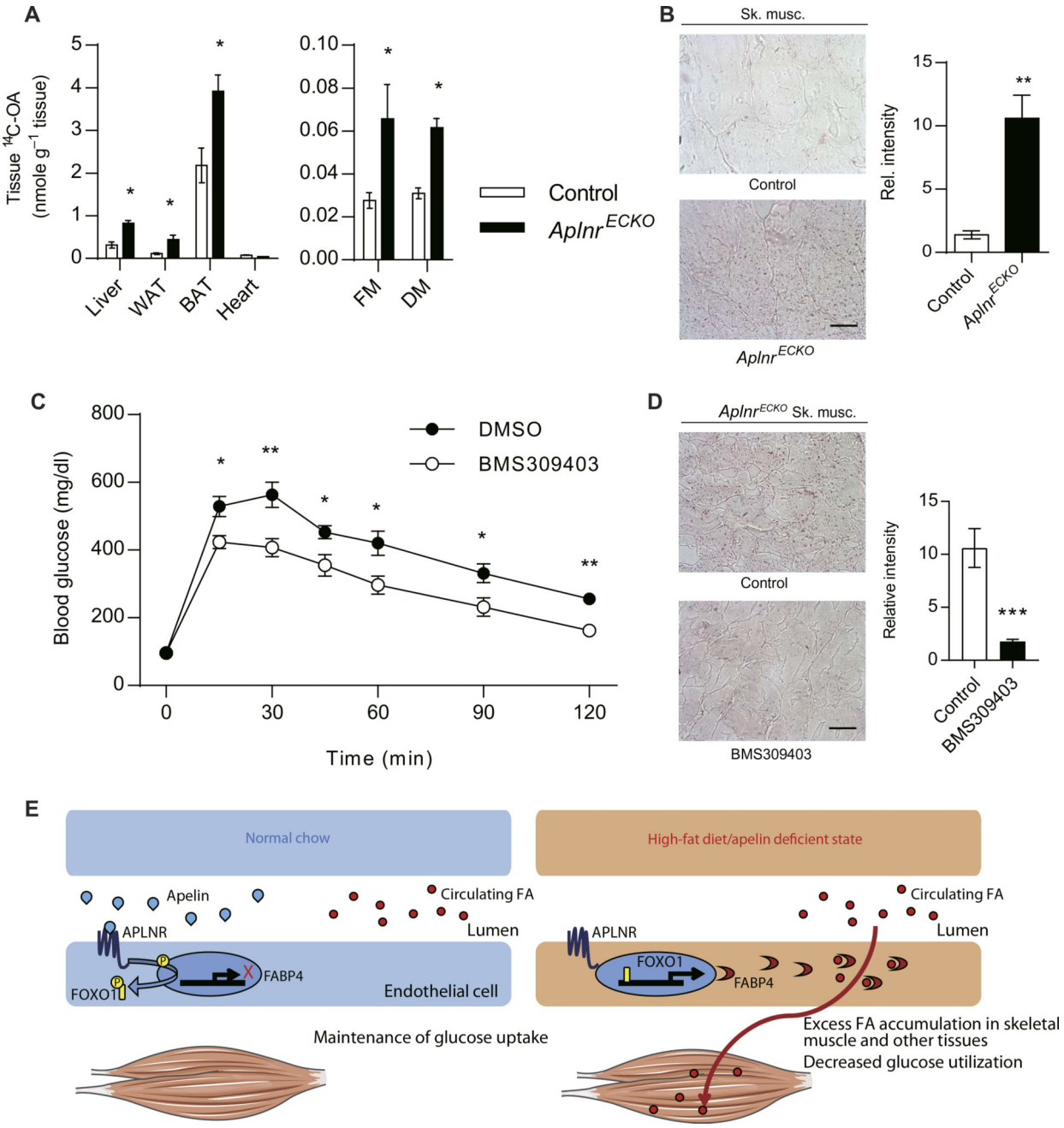

Fig. 6. Impaired glucose uptake of *Aplnr*^{ECKO} mice can be rescued by FABP4 inhibition

(**A**) Tissue uptake of ^{14}C-OA in the liver, WAT, BAT, heart, and skeletal muscle of *Aplnr*^{ECKO} mice at 24 hours after oral gavage (n = 5 per group). (**B**) Representative images and quantification of oil red O staining of skeletal muscle from *Aplnr*^{ECKO} mice and control littermates (n = 5 per group). Scale bar, 20 μm. (**C**) IPGTT in *Aplnr*^{ECKO} mice after 7 days of treatment with BMS309403 by oral gavage (n = 7 per group). (**D**) Representative images and quantification of oil red O staining of skeletal muscle from *Aplnr*^{ECKO} mice treated with

BMS309403 (n = 5 per group). Scale bar, 20 μm. (**E**) Proposed mechanism of endothelial apelin/APLNR metabolic signaling. *P < 0.05, **P < 0.01, and ***P < 0.001